SUPPLEMENT TO THE *WELDING JOURNAL*, JUNE 2012
Sponsored by the American Welding Society and the Welding Research Council

Strain-Age Cracking Susceptibility of Ni-Based Superalloys as a Function of Strain Rate, Temperature, and Alloy Composition

The influence of test temperature, strain rate, and alloy composition on cracking susceptibility of three Ni-based superalloys was examined

BY DAVID A. METZLER

ABSTRACT

Gamma-prime strengthened Ni-based superalloys comprise a family of critical construction materials for modern gas turbines used in land-based power-generation applications and aviation applications. Strain-age cracking during post-weld heat treatment (PWHT) remains a critical issue in the widespread use of higher-strength members of this alloy family. Previous work (Ref. 1) focused on development of a simple, Gleeble®-based controlled heating rate test method and specimen configuration that was used to compared the relative strain-age cracking susceptibility of several gamma-prime and gamma-double-prime forming alloys, especially in terms of their composition and total hardening phase precipitation capacity (volume fraction). This study, in contrast, investigated the effects of test temperature, strain rate, and alloy composition on strain-age cracking susceptibility using classic, response-surface DOE methods in temperature/strain-rate space, combined with elements of this previously developed experimental method. Observed results were rationalized in terms of known gamma-prime precipitation kinetics.

Introduction

Strain-age (reheat) cracking generally occurs in gamma-prime or gamma-double-prime-strengthened alloys during post-weld heat treatment (PWHT) or subsequent exposure of as-welded parts to elevated temperature service. Residual stresses, developed during restrained cooling, immediately following weld bead solidification or produced by differential thermal expansion during PWHT heat up are generally thought to be the driving force for cracking. Alloy matrix hardening during PWHT or subsequent service (through gamma-prime or gamma-double-prime precipitation) transfers the strains produced by these residual stresses onto the material's grain boundaries, with secondary grain boundary carbides often acting as crack initiation sites. Additionally, volume contraction associated with hardening phase precipitation, can provide additional stresses/strains that exacerbate cracking (Refs. 2, 4). This scenario, however, can only occur if hardening (by second-phase precipitation) proceeds more quickly than stress relief through recovery or recrystallization mechanisms.

Previous work (Ref. 1) documented the use of modified tensile specimen geometry and fixed thermomechanical test conditions to provide a means of comparing the strain-age cracking susceptibility of nickel-based superalloys. This Gleeble®-based controlled heating rate test (CHRT) method essentially locked in one "standard" heat-up rate through the gamma-prime precipitation temperature range, one fixed test temperature and extension rate within this temperature regime, chosen to represent a "grand average" of PWHT heat-up conditions for sheet and plate materials. In actual practice, PWHT heat-up rates may vary considerably, depending on part geometry and available heat treat furnace capability. The amount of time spent in the gamma-prime precipitation temperature range, roughly 1400°F (760°C) to 1600°F (871°C), may change from part to part, as well as the rate that residual stresses relax through part deformation (strain rate) during PWHT. Similarly, gamma-prime (or gamma-double-prime) precipitation kinetics and the total amount (volume fraction) of gamma-prime precipitated can vary considerably with alloy composition. Reported correlations between alloy composition and PHWT cracking have varied substantially, depending on the test methods used to assess strain-age cracking susceptibility (Refs. 4–6). This study represents an attempt to quantify the effects of different CHRT temperatures, extension (strain) rate at test temperature, and alloy equilibrium gamma-prime volume fraction/precipitation kinetics on the strain-age cracking response of three commercial gamma-prime hardened, Ni-based superalloys.

KEYWORDS

Reheat Cracking
Strain Rate
Superalloys
Ni-Based Alloys
Postweld Heat Treatment

Experimental Method

A classic Box-Behnken (face-centered cubic) response surface design was chosen for this study. The controlled heating rate test temperature, extension (strain) rate at test temperature, and alloy equilibrium gamma-prime volume fraction were selected as experimental inputs. Elongation to break, as a semiquantitative measure of strain-age cracking resistance, was the primary experimental response (output). The actual design contained 12 runs in one block with three replicated center points for experimental error assessment. This design is illustrated in Table 1.

Three common Ni-based superalloys were chosen for evaluation over the defined

DAVID A. METZLER is Senior Mechanical Metallurgist, Haynes International, Kokomo, Ind.

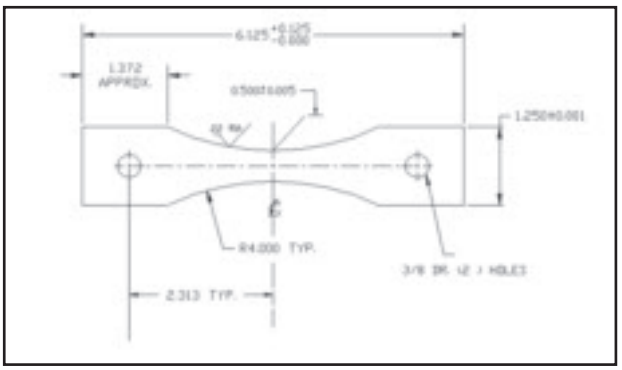

Fig. 1 — Specimen geometry used in CHRT response surface experiment.

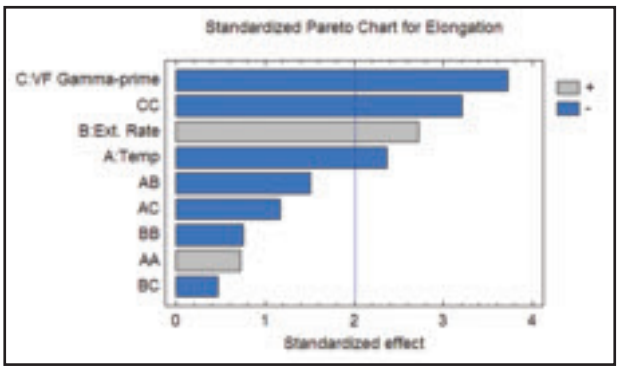

Fig. 2 — Pareto chart of main effects (vertical line represents 90% confidence level for statistical significance).

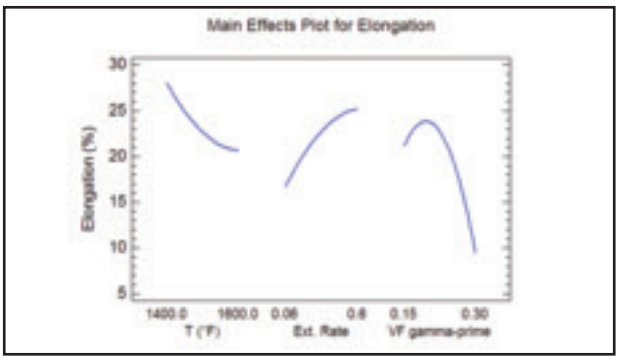

Fig. 3 — Main effects plot for CHRT elongation as function of temperature, extension rate, and equilibrium gamma-prime volume fraction.

range of modified CHRT conditions. All alloys were commercial gamma-prime strengthened materials. The end points of the gamma-prime volume fraction range were represented by alloys known to be relatively resistant (HAYNES® 263 alloy) and very susceptible (HAYNES® R-41 alloy) to strain-age cracking. These alloys and their compositions are listed in Table 2. Gamma-prime volume fraction was estimated from thermodynamic phase stability calculations performed with Pandat™ software and v7.0 of the Ni-Data database of thermodynamic properties published by Thermotech, Ltd. Calculations were performed at 931°F (500°C) to represent the maximum fraction of gamma-prime that each material could potentially precipitate (its "capacity" to precipitate gamma-prime). Other phases, expected to form at time scales well beyond CHRT test duration were suspended from the calculations (Ref. 1). Fortunately, the calculated equilibrium gamma-prime volume fraction for HAYNES® 282® alloy (0.240) fell close enough to the design value (0.225) to be usable without introducing excessive experimental error. This eliminated the need to employ a noncommercial alloy composition to "fill in" the equilibrium gamma-prime volume fraction midrange value.

The controlled heating rate test specimen blanks were cut from 0.063-in.- (1.69-mm-) thick mill annealed sheet, transverse to the final rolling direction, using a mechanical shear. (For gamma-prime strengthened alloys, the mill annealing cycle consists of a batch furnace anneal at the appropriate solution treatment temperature, followed by a water quench.) These blanks were finish machined to the dimensions depicted in Fig. 1 and Blanchard ground to remove the as-pickled sheet surface. A Type-K thermocouple was percussion welded at the mid-span of each specimen and 1-in. (25.4-mm) gauge marks were added to each specimen, centered at mid-span. This specimen geometry (Fig. 1) was designed (Ref. 1) to ensure that specimens fractured near mid-span when CHRT tested. These specimens were mounted in a PC-controlled Gleeble® 1500D between flat austenitic stainless steel jaws. A protective atmosphere was not used in these tests. Each specimen was heated to 1100°F (594°C) at 100°F (56°C) per second, then heated to the test temperature at 30°F (16.7°C) per minute. Each specimen was pulled to failure at the indicated extension rate. Elongation to failure was calculated from posttest measurements of the length increase between the 1-in. (25.4-mm) gauge marks. Tests were conducted in essentially random order, including the three center points.

After elongation measurement, a small longitudinal section (including the fracture surface) was cut from each specimen, mounted in epoxy, and prepared using standard metallographic techniques. Samples were first electrolytically etched with 5% oxalic acid in hydrochloric acid (HCl) for optical metallography, then re-prepared and re-etched (also electrolytically) with 15 g of chromic acid (CrO_3) plus 10 mL of concentrated sulfuric acid (H_2SO_4) dissolved in 150 mL of 85% phosphoric acid (H_3PO_4) (Ref. 3) before examination in a Zeiss Supra 40 SEM for evidence of gamma-prime precipitation.

Table 1 — CHRT Response Surface Experiment Design

Test Temperature °F (°C)	Extension Rate in./min (mm/min)	Estimated Alloy Gamma-Prime Volume Fraction
1500 (816)	0.332 (8.43)	0.225
1400 (760)	0.063 (1.60)	0.225
1600 (871)	0.063 (1.60)	0.225
1400 (760)	0.600 (15.2)	0.225
1600 (871)	0.600 (15.2)	0.225
1400 (760)	0.332 (8.43)	0.150
1600 (871)	0.332 (8.43)	0.150
1500 (816)	0.332 (8.43)	0.225
1400 (760)	0.332 (8.43)	0.300
1600 (871)	0.332 (8.43)	0.300
1500 (816)	0.063 (1.60)	0.150
1500 (816)	0.600 (15.2)	0.150
1500 (816)	0.063 (1.60)	0.300
1500 (816)	0.600 (15.2)	0.300
1500 (816)	0.332 (8.43)	0.225

Results

Controlled heating rate test results as a function of test temperature, extension rate, and estimated equilibrium gamma-prime volume fraction are listed in Table 3. A Pareto chart of the main effects is depicted in Fig. 2 and includes a 90% confi-

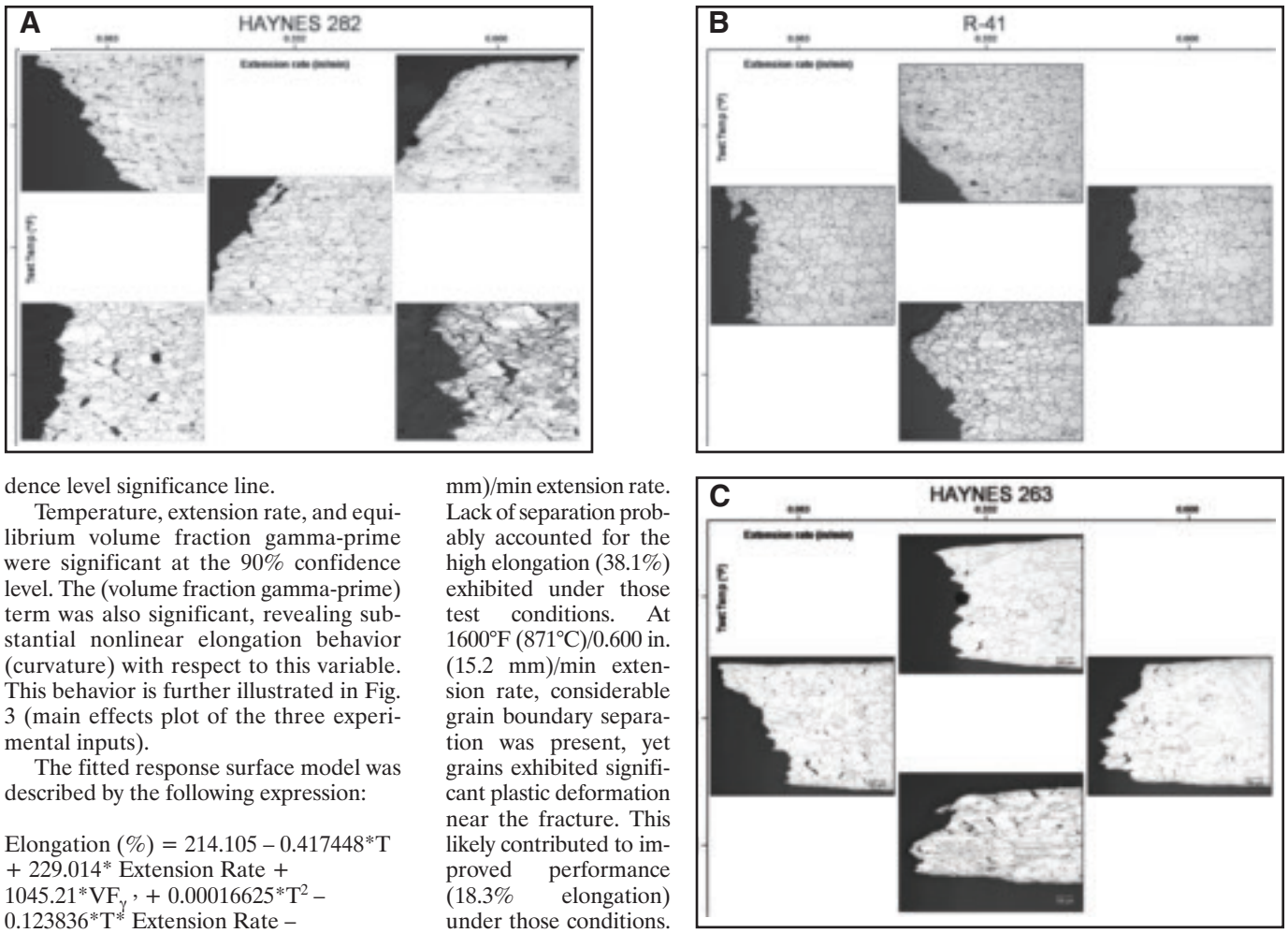

Fig. 4 — Post-CHRT microstructures at various temperatures (vertical axis) and extension rates (horizontal axis). A — 282; B — R-41 alloy; C — 263 alloy.

dence level significance line.

Temperature, extension rate, and equilibrium volume fraction gamma-prime were significant at the 90% confidence level. The (volume fraction gamma-prime) term was also significant, revealing substantial nonlinear elongation behavior (curvature) with respect to this variable. This behavior is further illustrated in Fig. 3 (main effects plot of the three experimental inputs).

The fitted response surface model was described by the following expression:

$$\text{Elongation } (\%) = 214.105 - 0.417448*T + 229.014* \text{ Extension Rate} + 1045.21*VF_{\gamma}{}' + 0.00016625*T^2 - 0.123836*T* \text{ Extension Rate} - 0.343333*T* VF_{\gamma}{}' - 24.1011* \text{ Extension Rate}^2 - 50.9001* \text{ Extension Rate} * VF_{\gamma}{}' - 1313.33* VF_{\gamma}{}'^2$$

(T in °F, Extension Rate in in./min.; $VF_{\gamma}{}'$ = equilibrium volume fraction of gamma-prime by thermodynamic calculation.)

This model exhibited a correlation coefficient (R^2) of 0.89 (0.70, adjusted for degrees of freedom). Although the interaction terms were included in the regression equation, none of these terms were statistically significant and can be dropped from the model with little loss of accuracy, giving the following:

$$\text{Elongation } (\%) = 23.9457 + 512.905* VF_{\gamma}{}' + 15.8287* \text{ Extension Rate} - 0.037*T - 1312.38* VF_{\gamma}{}'^2$$

This simplified model also exhibited an adjusted (for degrees of freedom) R^2 of 0.70.

Optical Metallography

An overview of microstructures produced by CHRT within the experimental envelope described above is contained in Fig. 4A–C. In 282, grain boundary separation was present in all samples except those tested at 1400°F (760°C)/0.600 in. (15.2 mm)/min extension rate. Lack of separation probably accounted for the high elongation (38.1%) exhibited under those test conditions. At 1600°F (871°C)/0.600 in. (15.2 mm)/min extension rate, considerable grain boundary separation was present, yet grains exhibited significant plastic deformation near the fracture. This likely contributed to improved performance (18.3% elongation) under those conditions. No significant amount of secondary carbide precipitation was found in post test specimen grain boundaries.

R-41 test specimens exhibited little evidence of plastic deformation under all test conditions, except at the fracture surface, itself. This was only observable at the

Table 2 — Composition of Alloys Used for Response Surface Experiment

Alloy	R-41	HAYNES® 282	HAYNES® 263
Element	wt-%	wt-%	wt-%
Al	1.49	1.46	0.57
B	0.01	0.00	0.00
C	0.09	0.06	0.06
Co	10.69	10.11	19.91
Cr	19.42	19.67	19.91
Cu	0.01	0.00	0.00
Fe	3.72	0.20	0.36
Mn	0.01	0.04	0.41
Mo	9.91	8.36	5.77
Si	0.05	0.04	0.23
Ti	3.11	2.08	2.19
V	0.02	0.01	0.00
W	0.05	0.00	0.00
Nb	0.00	0.00	0.00
Ni	51.43	57.97	50.59
Estimated Gamma Prime Volume Fraction at 931°F (500°C)	0.30	0.24	0.15

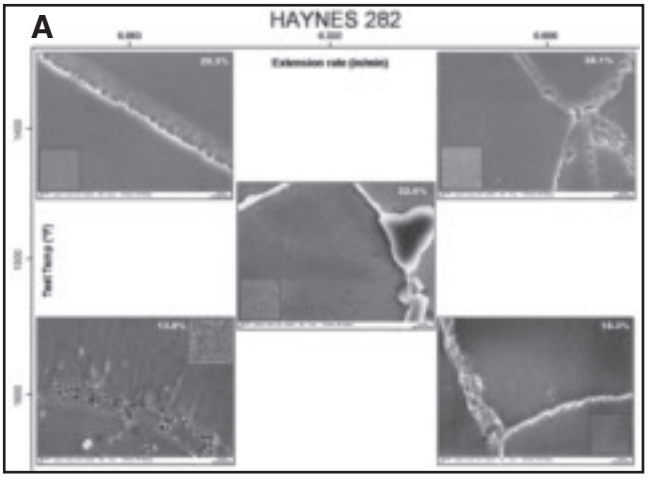

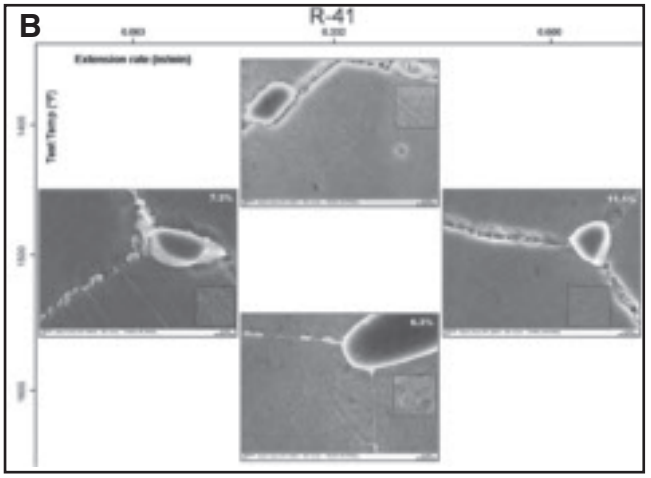

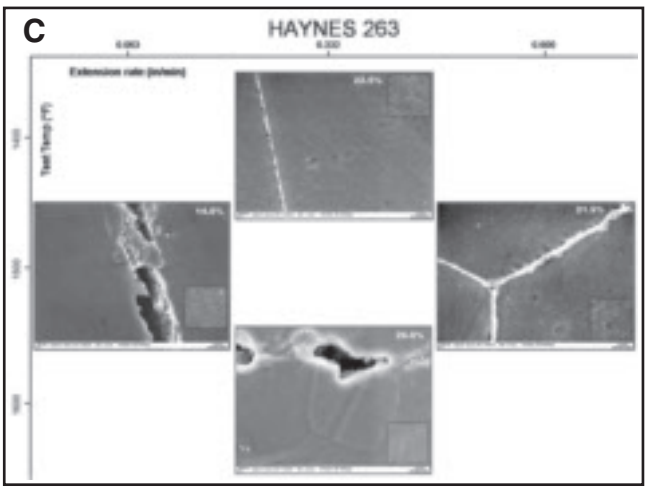

Fig. 5 — Post-CHRT microstructures at high magnification at various temperatures and extension rates. Inset magnified 2×. (CHRT test elongations shown on micrographs.). A — 282 alloy; B — R-41 alloy; C — 263 alloy.

1400°F test temperature. Specimens tested at higher temperatures exhibited only intergranular failure. The grain boundaries in this alloy contained a nearly continuous film of secondary carbide precipitation after testing at all temperature/extension rate conditions. (This film was not present in pretest microstructures.) The formation of these continuous grain boundary carbide films probably provided a low-energy fracture propagation path along the grain boundaries. This, coupled with a partially gamma-prime hardened matrix, likely exacerbated intergranular fracture beyond that normally encountered in Ni-based alloys in this temperature range.

Alloy 263 exhibited grain boundary separation at all test temperatures. Only minor amounts of plastic deformation were found at 1400°F and 1500°F (816°C). At 1600°F (871°C), this alloy contained significant grain elongation and some dynamic recrystallization after testing at 0.332 in. (8.43 mm)/min even though significant grain boundary separation had occurred. As expected, this specimen showed (relatively) high elongation (26.0%) to failure. No significant amount of secondary carbide precipitation was found in posttest specimen grain boundaries.

Electron (SEM) Metallography

Some early investigators (Ref. 7) questioned whether gamma-prime actually precipitated during a similar test regime in Inconel® X-750 alloy. To address this question, post CHRT specimens were also examined by SEM for signs of gamma-prime precipitation, especially in areas adjacent to grain boundaries that had clearly separated. A different etchant (described above) was used to reveal gamma-prime particles in relief. An overview of these structures is illustrated in Fig. 5A–C.

Gamma-prime particles were not visible in 282 alloy after 1400°F testing at any extension rate. At 1500°F/0.332 in. (8.43 mm)/min, some very fine, gamma-prime appeared to have precipitated in grain interiors. Some blocky carbides were also

Table 3 — CHRT Results, Box-Behnken Response Surface Experiment

Test Temperature °F (°C)	Extension Rate in./min (mm/min)	Estimated Gamma-Prime Volume Fraction	Elongation to Failure 1-in. (25.4-mm) Gauge Marks	Pretest GS (ASTM)	Posttest GS (ASTM)
1500 (816)	0.332 (8.43)	0.225	23.4	4.0	4.0
1400 (760)	0.063 (1.60)	0.225	20.3	4.0	3.5
1600 (871)	0.063 (1.60)	0.225	13.8	4.0	3.5
1400 (760)	0.600 (15.2)	0.225	38.1	4.0	4.0
1600 (871)	0.600 (15.2)	0.225	18.3	4.0	4.0
1400 (760)	0.332 (8.43)	0.150	22.5	3.5	3.5
1600 (871)	0.332 (8.43)	0.150	26.0	3.5	DRX?
1500 (816)	0.332 (8.43)	0.225	22.2	4.0	4.0
1400 (760)	0.332 (8.43)	0.300	13.1	6.0	6.0
1600 (871)	0.332 (8.43)	0.300	6.3	6.0	6.0
1500 (816)	0.063 (1.60)	0.150	14.0	3.5	3.5
1500 (816)	0.600 (15.2)	0.150	21.9	3.5	3.5
1500 (816)	0.063 (1.60)	0.300	7.3	6.0	6.0
1500 (816)	0.600 (15.2)	0.300	11.1	6.0	6.0
1500 (816)	0.332 (8.43)	0.225	22.5	4.0	4.0

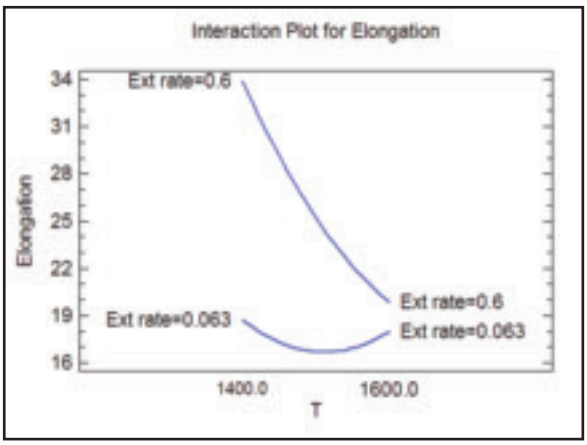

Fig. 6 — Extension rate/test temperature interaction plot.

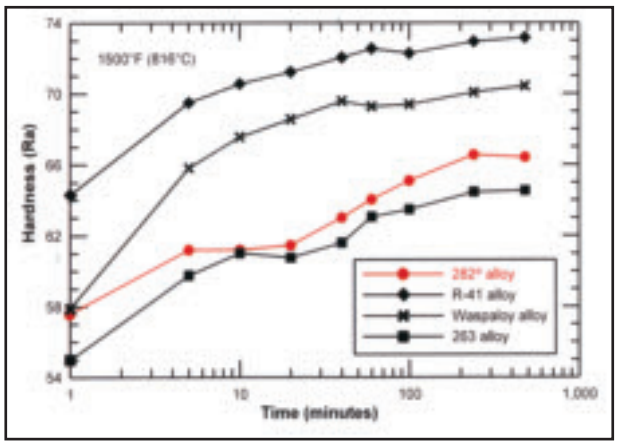

Fig. 7 — Comparative age-hardening kinetics of several wrought gamma-prime-strengthened alloys (Ref 8).

found in grain boundaries. At 1600°F/ 0.063 in. (1.60 mm)/min, gamma-prime clearly had formed during heat up and testing. Small, secondary carbide particles had also precipitated in grain boundaries. The presence of these smaller, but noncontinuous grain boundary carbides would not likely reduce grain boundary ductility to the degree that a continuous secondary carbide film would. A gamma-prime denuded zone was present near grain boundaries where secondary carbide precipitation had occurred. At the higher extension rate, 0.600 in. (15.2 mm)/ min, no gamma-prime particles were visible in posttest specimens.

Gamma-prime particles were clearly present in R-41 over the entire range of test conditions. Grain boundaries contained nearly continuous deposits of small secondary carbides and numerous, larger blocky carbides, often located at grain boundary triple points. No gamma-prime denuded zones were apparent near grain boundaries. As expected, higher test temperatures and slower extension rates (more time at test temperature) yielded lower elongations during CHR testing. Gamma-prime particles were more easily distinguished following tests that yielded the lowest elongations.

Posttest gamma-prime appeared to be present in 263 alloy under all conditions except 1600°F/0.332 in. (8.43 mm)/min. These test conditions also produced partial dynamic (or meta-dynamic) recrystallization, again suggesting that significant gamma-prime precipitation had not occurred. These conditions also yielded the highest elongation in the entire test matrix. Although some large, blocky carbides were present in grain boundaries, their presence would not likely reduce the observed CHRT elongation significantly because they did not form a continuous film ("easy" fracture path). Discreet, secondary carbide, grain boundary precipitates were not generally resolvable.

Discussion

DOE Analysis

Standardized main effects results produced by this response surface experiment showed that volume fraction gamma-prime, test temperature, and extension rate were significant at the 90% confidence level. As expected (qualitatively), higher extension rates favored higher test elongation results, simply by reducing the total amount of time specimens spent in the gamma-prime precipitation temperature regime. The magnitude of this effect did not change significantly with alloy identity. (The gamma-prime volume fraction/extension rate interaction was not statistically significant.)

Similarly, higher test temperatures generally favored lower test elongation results. Although the temperature/extension rate interaction fell just below statistical significance (at the 95% CL), it was the largest two-factor interaction yielded by this experiment and is illustrated in Fig. 6.

This plot suggests that at high extension rates, temperature plays a more important role than at low extension rates. At the "standard" CHRT extension rate, 0.063 in. (1.60 mm)/min, test behavior appears to vary little with temperature (in the gamma-prime precipitation regime). Test time may be long enough such that alloy gamma-prime precipitation capability (gamma-prime equilibrium volume fraction) becomes dominant over short-term precipitation kinetics. At higher extension rates, thermally activated precipitation kinetics limit the rate at which elongation decreases during CHRTs.

The main effect of equilibrium gamma-prime volume fraction on CHRT elongation was strongly significant. Its second-order effect was also statistically significant, indicating strong nonlinear CHRT elongation vs. equilibrium gamma-prime volume fraction behavior. The main effects plot (contained in Fig. 3, right-hand curve) illustrates this behavior. Alloy 282, whose calculated equilibrium gamma-prime volume fraction was 0.24, exhibited anomalously high CHRT elongations. The sluggish gamma-prime precipitation rate characteristic of this alloy (Fig. 7) apparently limits the amount of elongation reduction under all CHRT conditions visited in this experiment, as opposed to R-41 and 263, where equilibrium gamma-prime volume fraction primarily controls CHRT behavior.

These DOE results are also supported by the SEM microstructural observations conducted in this study. Post-CHRT R-41 specimens contained observable gamma-prime particles over the entire temperature/extension rate space of this experiment. Similarly, 263 post-CHRT specimens contained observable gamma-prime particles, except at the highest test temperature, 1600°F. In contrast, gamma-prime particles were only observable in 282 alloy at the highest test temperature and lowest extension rate.

Conclusions

1) The CHRT (strain-age cracking) response of several gamma-prime hardenable Ni-based superalloys can be described in terms of a simple quadratic model in test temperature, extension rate, and equilibrium volume fraction gamma-prime (alloy composition) space as follows:

$$\text{Elongation } (\%) = 23.9457 + 512.905 * VF_{\gamma'} + 15.8287 * \text{Extension Rate} - 0.037 * T - 1312.38 * VF_{\gamma'}^{2}$$

2) Test temperature and extension rate effects behaved linearly; their exhibited curvature was less than observed experimental error. The CHRT elongation de-

creased with increasing test temperature and increased with extension rate.

3) The effect of equilibrium gamma-prime volume fraction was strongly nonlinear, with the 282 alloy exhibiting anomalously large CHRT elongations.

4) This nonlinear behavior appears to be caused by 282's sluggish gamma-prime precipitation kinetics relative to the R-41 and 263 alloys. The R-41 and 263 alloys developed observable gamma-prime particles under almost all test conditions visited in this study, while 282 only exhibited observable precipitation at the highest test temperature and low extension rates.

5) The overall CHRT behaviors of the 41 and 263 alloys are determined more by the total amount of gamma prime that can potentially precipitate (alloy composition) than precipitation kinetics, whereas in 282 alloy, sluggish precipitation kinetics dominate its CHRT response.

6) All fabrication history gathered to date on the 282 alloy has indeed suggested that this alloy is quite resistant to strain-age cracking.

Acknowledgments

Lori Meacham, John Cotner, and Mark Richeson of Haynes International are gratefully acknowledged. Meacham assisted with Gleeble-based CHRT operation and programming. Cotner and Richeson provided electron and optical metallography skills necessary to complete this study.

References

1. Metzler, D. A. 2008. A Gleeble®-based method for ranking the strain-age cracking susceptibility of Ni-based superalloys. *Welding Journal* 87(10): 249-s to 256-s.

2. C. T. Sims, and W. C. Hagel, eds. 1972. *The Superalloys*, pp. 529–531, New York, N.Y., Wiley.

3. Radavich, J. F. 1997. Electron metallography of alloy 718. *Superalloys 718, 625, 707 and Various Derivatives,* E. A. Loria, ed. The Minerals, Metals and Materials Society, pp. 17–18.

4. Norton, S. J., and Lippold, J. C. 2003. Development of a Gleeble-based test for postweld heat treatment cracking susceptibility. *Trends in Welding Research, Proc. of the 6th International Conference*, ASM International, pp. 609–614.

5. Prager, M., and Shira, C. S. 1968. Welding of precipitation hardenable nickel-base alloys. *WRC Bulletin No. 128.*

6. Rowe, M. D. 2006. Ranking the resistance of wrought superalloys to strain-age cracking. *Welding Journal* 85(2): 27-s to 34-s.

7. Dix, A. W., and Savage, W. F. 1971. Factors influencing strain-age cracking in Inconel X-750. *Welding Journal* 50(6): 247-s to 252-s.

8. HAYNES® 282® brochure, *www.haynesintl.com/pdf/h3173.pdf,* p. 10.

Correction

One author's name was misspelled for the paper titled Design of Experiment and Goal Programming Application for the GMAW Process, which ran in the April issue of the *Welding Journal* Research Supplement beginning on page 106-s. The correct spelling is N. E. İpek. The names of the four authors are Y. T. IÇ, F. ELALDI, F. PAKDIL, and N. E. İPEK.

The *Welding Journal* apologizes for the error.